13th International Symposium on Turbulence and Shear Flow Phenomena (TSFP13)
Montreal, Canada, June 25–28, 2024

SELF-SIMILAR PROPERTIES OF THE REYNOLDS SHEAR STRESS PROBABILITY DISTRIBUTION IN WALL-BOUNDED FLOWS

Spencer Zimmerman
Department of Mechanical Engineering
Stony Brook University
Stony Brook, NY 11794, USA
spencer.zimmerman@stonybrook.edu

Jimmy Philip
Department of Mechanical Engineering
University of Melbourne
Parkville, Victoria 3010, Australia
jimmyp@unimelb.edu.au

Yoshinobu Yamamoto
Department of Mechanical Systems Engineering
University of Yamanashi
Takeda, Kofu, Yamanashi, 400-8510, Japan
yamamotoy@yamanashi.ac.jp

Yoshiyuki Tsuji
Department of Energy Engineering and Science
Nagoya University
Chikusa-ku, Furo-cho, 464-8603, Japan
c42406a@nucc.cc.nagoya-u.ac.jp

Joseph Klewicki
Department of Mechanical Engineering
University of Melbourne
Parkville, Victoria 3010, Australia
klewicki@unimelb.edu.au

ABSTRACT

Probability distributions of the normalized Reynolds shear stress (RSS) and joint cumulants of the normalized streamwise and wall-normal velocity components up to sixth order are presented spanning over three decades of friction Reynolds numbers Re_τ in several wall-bounded flows. It is shown that the fourth-order joint cumulants are non-zero and essentially invariant with Reynolds number for $Re_\tau \gtrsim 2000$ despite changes in the correlation coefficient between the two velocity components. Several sixth order joint cumulants are also non-zero and appear to become invariant with Reynolds number, albeit more slowly than the fourth-order ones. This indicates that the interactions between the streamwise and wall-normal velocities do not become reducible to those implied by their second-order moments (i.e. their covariance matrix) with increasing Reynolds number, but also that the Reynolds number dependence of the RSS distribution (at least out to a substantial number of standard deviations) is attributable almost entirely to that of the second-order moments. The fidelity of a model distribution given by Antonia & Atkinson (*J. Fluid Mech.*, vol. 58, 1973, pp. 581–593) that includes the effects of cumulants up to 4th order is also evaluated against the experimental data. It is shown that this distribution is accurate to roughly 25 times the mean RSS in the negative tail and 15 times the mean RSS in the positive tail. Beyond this, the model distribution predicts negative probabilities in the negative tail when the present experimental cumulant values are inputted, and thus a higher order expansion is necessary if one aims to obtain a general model distribution equation for the RSS.

INTRODUCTION

Self-similarity is a central concept underlying several noteworthy models of wall-bounded turbulent flows, including those stemming from the attached eddy hypothesis (e.g. Townsend (1976), Perry & Chong (1982)) mean-momentum-balance (MMB) analysis (Fife *et al.*, 2005) and resolvent mode analysis (e.g. McKeon & Sharma (2010), Moarref *et al.* (2013)). Owing to its connection to the mean velocity (via the MMB), the Reynolds shear stress (RSS) in particular represents both a likely exhibitor of self-similarity in the log-layer as well as an attractive modeling target for its exploitation. Indeed, MMB analysis reveals that self-similarity of the mean dynamics (i.e. invariant properties of the RSS profile) is inextricably linked to distance-from-the-wall scaling and thus to the logarithmic mean velocity profile. With self-similarity properties of the mean RSS profile fairly well characterized, we turn our attention at present to the fluctuations in an effort to better understand the degree to which this self-similarity is reflected in the turbulent fluctuations.

Markers of self-similarity in a fluctuating signal may include those relating to the length/time scales and those relating to signal magnitude. The former may be uncovered via analysis of energy distribution across various modes (e.g. Fourier or proper orthogonal modes, Hellström & Smits (2017)), structure functions, or zero-crossing length distributions (Morrill-Winter *et al.*, 2017*b*), while the latter may be uncovered via analysis of the probability distributions, including interrogation of moment profiles (e.g. mean, variance, skewness, kurtosis) (Zimmerman *et al.*, 2019), cumulant profiles (Antonia & Atkinson (1973), Nakagawa & Nezu (1977)) or Kullback-Leibler divergence Lindgren *et al.* (2004) (or similar) from a reference distribution. Here we will focus on manifesta-

tions of self-similarity in the fluctuation magnitude by decomposing the probability distribution into 'product-of-Gaussians' and non-'product-of-Gaussians', or PoG and non-PoG, components. The PoG component is self-similar by construction at fixed correlation coefficient r, and thus departures from self-similarity will be captured purely by changes in the non-PoG component of the distribution.

Table 1. Summary of the present datasets. M06 collectively refers to Del Alamo & Jiménez (2003), Del Alamo *et al.* (2004) and Hoyas & Jimenez (2006), YT18 refers to Yamamoto & Tsuji (2018), Z19 refers to Zimmerman *et al.* (2019), MW17 refers to Morrill-Winter *et al.* (2017*a*), and P04 refers to Priyadarshana (2004). † See text for details concerning DNS turnover 'times'.

Dataset	Flow	Re_τ $(\cdot 10^3)$	Ut_s/δ $(\cdot 10^3)$
M06	Channel	0.5–2	23–46†
YT18	Channel	1–8	0.16†
Z19	TBL/Pipe	5–10	5–25
MW17	TBL	2–16	1.6–103
P04	ASL	$\sim$1000	~ 0.1

DATASETS

Data for the present analysis were aggregated from several earlier studies, including the channel DNS of Hoyas & Jimenez (2006) (HJ06) and Yamamoto & Tsuji (2018) (YT18), the laboratory hotwire measurements of Morrill-Winter *et al.* (2017*a*) (MW17) and Zimmerman *et al.* (2019) (Z19), and the atmospheric surface layer (ASL) hotwire measurements of Priyadarshana (2004) (P04). The Z19 and MW17 datasets each contain measurements from the Flow Physics Facility (FPF) (Vincenti *et al.*, 2013) as well as the Melbourne Wind Tunnel (MWT) Marusic *et al.* (2015), while Z19 also contains measurements from the Center for International Collaboration in Long Pipe Experiments (CICLoPE) (Talamelli *et al.*, 2009). The Reynolds number ranges and sample lengths (measured in number of boundary layer turnovers) of these studies are given in table 1.

The DNS fields associated with Del Alamo & Jiménez (2003), Del Alamo *et al.* (2004), and Hoyas & Jimenez (2006) (hereafter referred to as M06 or the 'Madrid DNSs') measured $(8\pi \times 4\pi)\delta$, $(8\pi \times 3\pi)\delta$, and $(8\pi \times 3\pi)\delta$ respectively in their streamwise-spanwise extent, where δ is the channel half-height. These DNS fields were probed for statistics at full resolution in x and $(\pi/100)\delta$ intervals in z for between $3-6$ snapshots for each of the three Reynolds numbers studied. The DNS fields from Yamamoto & Tsuji (2018) were each probed across the full simulation domain of $(16.0 \times 10)\delta$ in streamwise-spanwise extent for a duration of approximately 160 half-height turnovers. The low number of boundary layer turnovers for the ASL case is primarily due to the 60–90m boundary layer thickness rather than an abnormally short recording time. The distributions associated with the ASL dataset appear more converged for the limited number of turnovers than would the lower Reynolds number data at the same number of turnovers, but we cannot rule out a potential effect of under-converged contributions from very large scale motions (i.e. $O(100\delta)$) that are known to contribute to the RSS (Guala *et al.*, 2006). The hotwire arrays used to collect the ASL data were held between 18–50cm from the ground, which would put them at $y^+ = O(10^3)$–$O(10^4)$ (superscipt '+' denotes normalization by the wall shear scales), well within the logarithmic layer. Taken together, the distributions presented herein span a considerable range of Reynolds numbers and fluctuation strengths (i.e. 'tail' probabilities) compared to those shown in Antonia & Atkinson (1973), whose work we aim to extend.

CUMULANTS

We begin by presenting the expression originally derived by Antonia & Atkinson (1973) for the probability distribution of the product of two random variables with unit variance in terms of their joint cumulants k_{jk}. Here the two random variables are the fluctuating streamwise and wall-normal velocities normalized by their standard deviations, or $u_\sigma \equiv u/\sigma_u$ and $v_\sigma \equiv /\sigma_v$, and their product is $w \equiv u_\sigma v_\sigma$. This makes the mean value of w equal to the RSS correlation coefficient, i.e. $\langle w \rangle = r$. The subscripts j and k respectively represent the order of the streamwise and wall-normal velocities in the joint cumulant as well as the standard joint moments $m_{jk} \equiv \langle u_\sigma^j v_\sigma^k \rangle$. The expression given by Antonia & Atkinson (1973), derived from a generalized Gram-Charlier expansion of the joint PDF of u_σ and v_σ up to order four, is as follows:

$$p_w(w) = \frac{\exp\left[\frac{rw}{1-r^2}\right]}{\pi\sqrt{1-r^2}} \left\{ K_0\left(\frac{|w|}{1-r^2}\right)\left[1 + aw^2 + bw + c\right] - \frac{|w|}{1-r^2} K_1\left(\frac{|w|}{1-r^2}\right)[dw+e] \right\} \quad (1)$$

where K_0 and K_1 are modified Bessel functions of the second kind of order 0 and 1 respectively. The polynomial coefficients a, b, c, d, and e are each comprised of rational polynomials in r with coefficients dependent on groups of summed fourth-order terms of the form $D_{ij} \equiv k_{jk}/j!k!$ (e.g. with coefficients like $D_{31} + D_{13}$ or $D_{40} + D_{22} + D_{04}$, see equation (12) in Antonia & Atkinson (1973) for details). If the fourth order cumulants are zero, then so too are the coefficients a–e, and thus (1) reduces to the equation for the PDF of the product of two jointly-normal dependent variables. Note that all cumulants above 2nd order are zero for Gaussian/multivariate normal distributions.

The above formulation invites an interpretation of high-order cumulants as relating to the 'non-Gaussian' components of the underlying random variables. This is not, however, the complete picture. Moments of multivariate normal distributions are always expressible in terms of covariances alone (i.e. second order moments) (Isserlis, 1918), whereas the cumulant k_{jk} quantifies the contributions to m_{jk} that are not attributable to *any* lower-order interactions. Thus, a joint distribution for which all 6th order cumulants were zero would not necessarily indicate 'Gaussianity' of the 6th order moments, but rather that m_{33} (for example) could be expressed in terms of lower order moments such as $m_{30}m_{03}$ (in addition to covariance terms). This property is also illustrated by the following relationships between m_{jk} and k_{jk} (for zero-mean, unit variance variables), which are given up to order 6 in accordance with the analysis

to follow:

$$
\begin{aligned}
k_{40} &= m_{40} - (3) \\
k_{31} &= m_{31} - (3r) \\
k_{22} &= m_{22} - (2r^2 + 1) \\
k_{60} &= m_{60} - (15m_{40} + 10m_{30}^2 - 30) \\
k_{51} &= m_{51} - (5m_{40}r + 10m_{30}m_{21} + 10m_{31} - 30r) \\
k_{42} &= m_{42} - (m_{40} + 4m_{30}m_{12} + 6m_{22}^2 + 6m_{21}^2 + 8m_{31}r \\
&\qquad -24r^2 - 6) \\
k_{33} &= m_{33} - (m_{30}m_{03} + 9m_{21}m_{12} + 9m_{22}r + 3m_{31} + 3m_{13} \\
&\qquad -12r^3 - 18r)
\end{aligned}
\tag{2}
$$

Here the terms in the parentheses amount to factorizations of the corresponding moment m_{jk} outside the parentheses into products of lower order moments. Note that all terms would have subscripts that sum to the corresponding order of the cumulant, but that $m_{11} = r$, and $m_{20} = m_{02} = 1$ are used for brevity. Note further that the coefficients in (2) can be checked by setting $u_\sigma = v_\sigma$ and assuming Gaussianity so that $r = 1$, $m_{jk} = 0$ when $j+k$ is odd, $m_{jk} = 3$ when $j+k = 4$, and $m_{jk} = 15$ when $j+k = 6$.

RESULTS

As noted in the previous section, the fourth order cumulants appear in equation (1) in the form $D_{jk} \equiv k_{jk}/j!k!$. Scaling by the factorials of the component orders is therefore the appropriate way to compare the magnitude of one cumulant to the next in the context of their effects on the probability distribution. Profiles of these scaled cumulants along with the correlation coefficient r are plotted in the left column of figure 1, while individual values taken from the outer edge of the log layer ($y/\delta \approx 0.1$) are plotted against Reynolds number in the right column of figure 1. The cumulant profiles in the left column are grouped by dataset, and shifted vertically relative to one another for clarity. The ordinate scale of the profiles is linear with a magnitude indicated by the bottom two tick labels. The total range of the cumulant profile plots in figure 1 is 0.25 with each successive dataset shifted up by 0.05, while the total range of the correlation coefficient profile plots is 1.2 with each successive dataset shifted up by 0.2.

Inspection of the profile plots in figure 1 reveals that all five of the fourth order cumulants tend to plateau in the log-layer in sharp contrast to their behavior in the wake and buffer layers. Within each dataset, darker shaded lines and symbols represent higher Reynolds numbers. While this allows rough Reynolds number trends to be observed in some cases, picking off the values of these profiles at the approximate outer edge of the log-layer allows for a closer inspection of these trends. For all fourth-order cumulants, there is considerably more systematic variation between the three Madrid channel DNS cases than is observed amongst the laboratory datasets. This can be seen from the profiles in the left column to be the result of the emergence of a distinct overlap region between the near-wall and wake regiones (i.e. a log-layer for the mean velocity). The highest Reynolds number DNS case does exhibit a distinct overlap layer, and as a result is in excellent agreement with the experimental data at similar Reynolds numbers. For the next decade change in friction Reynolds number δ^+ there is far less variation, as the overlap layers have emerged and the plateaus essentially developed. Bearing in mind the uncertainty and potential under-convergence of the ASL cases in the extreme Reynolds number regime, all five fourth-order cumulants appear to become essentially invariant once this overlap layer emerges around $\delta^+ = 2000$. This is not the case, however, for the correlation coefficient. The correlation coefficient decreases steadily across the complete range of Reynolds numbers presented, which in light of the fact that $\langle uv \rangle^+ \approx 1$ at this location indicates that one or both of u_σ^+ and v_σ^+ are increasing with δ^+. Whether or not r eventually reaches a plateau is unresolved, with some models suggesting u_σ^+ is unbounded in the limit of infinite Reynolds number (Marusic & Kunkel, 2003) and others suggesting it eventually saturates (Chen & Sreenivasan, 2022).

Probability densities of three cases are plotted in figure 2 along with the model given by equation (2) using the measured values r and k_{jk}. The three densities shown correspond to the $y/\delta = 0.1$ locations taken from the $\delta^+ = 934$ M06 channel DNS and the $\delta^+ = 7700$ Z19 pipe experiment, and the log-layer location from the $\delta^+ \approx 890{,}000$ P04 ASL experiment. Note that the location of the ASL cases are known with less certainty as δ was not measured directly, but that they are well within the log-layer and $y^+ = O(10^3)$–$O(10^4)$. These three cases are selected as they span a wide Reynolds number range, but do not reflect any behavior that is not also present in the other measurements. The distributions show that increasing Reynolds number has the effect of increasing the probability density of very large positive RSS events but very little effect on that of the large negative RSS events. Although difficult to see in figure 2, there is cumulatively a large shift in probabilities from negative to positive events within the range $|w| < 5$ with increasing Reynolds number, which largely accounts for the correlation coefficient becoming more positive. This effect can also be seen in (1), where the prefactor that is proportional to $\exp(rw)$ can be visualized in terms of a multiplication of the otherwise symmetric Bessel functions by a line of slope $\propto r$ when plotted on a logarithmic ordinate. Overall, negative events decrease in likelihood from 64.3% for the DNS case at $\delta^+ = 934$ to 59.6% for the ASL case at $\delta^+ \approx 890{,}000$, with over 97% of that shift attributable to the range $|w| < 5$.

The Reynolds number dependencies observed in the context of figure $2(a)$ are almost entirely attributable to changes in the correlation coefficient. This fact is illustrated by figure $2(b)$ which shows the ratio of each PDF in figure 2 to the joint-normal distribution having the same correlation coefficient but zero cumulants. In this representation, the joint-normal distributions are the horizontal dashed lines with magnitude 1, but note that successive cases are shifted up by a decade for visibility. Despite clear changes to the shape and tail behavior of the measured probability distributions, all three cases show remarkably similar behavior relative to their equivalent joint-normal distributions. This further illustrates the degree of 'invariance' of the cumulants discussed above. It is also clear that this invariance is not due to lack of influence of these cumulants on the distribution, as the curves computed from equation (2) peel away from the joint-normal dashed lines (and track the measured distributions) for positive events exceeding about 5 times the mean RSS magnitude. Inclusion of the fourth order cumulants produces a faithful description of the PDF for events ranging in magnitude from about -25 to 15 times the mean RSS magnitude, whereas the assumption of joint normality is particularly poor for positive events greater than about 5 times the mean RSS magnitude. One issue with (1), however, concerns the behavior of extremely high magnitude negative events. Closer inspection of equation 12 in Antonia & Atkinson (1973) reveals that this expression will predict negative probabilities when $(D_{13} + D_{31}) > (D_{40} + D_{04} + D_{22})$,

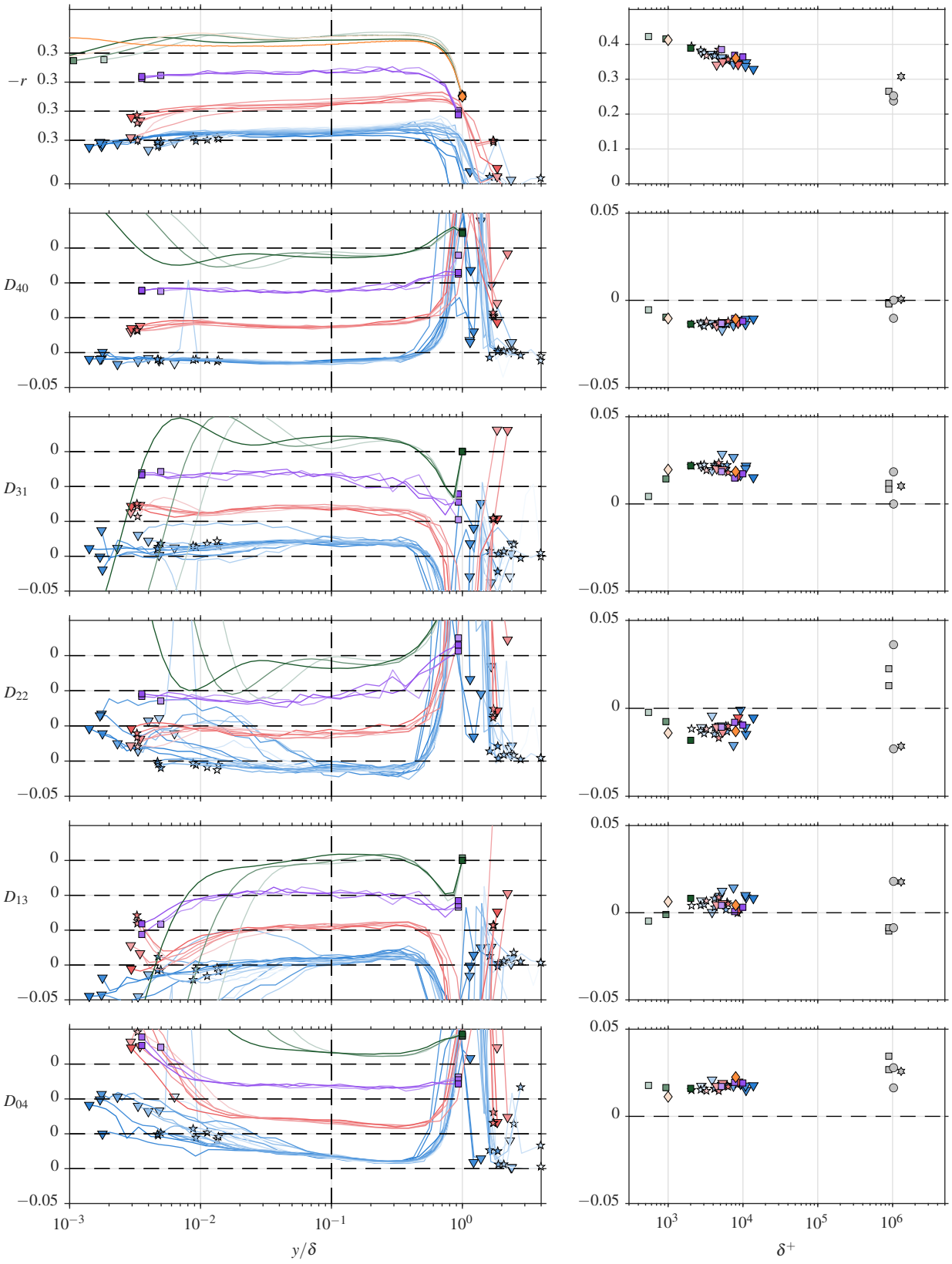

Figure 1. Left: Profiles of RSS correlation coefficient and scaled fourth order joint cumulants $D_{jk} \equiv k_{jk}/j!k!$ of the streamwise and wall-normal velocities for several datasets. Datasets are grouped by study and flow type, and are assigned a color along with a vertical shift for visibility. Darker colors indicate higher Reynolds number. MW17 FPF (▽), MW17 MWT (☆), Z19 FPF (▽), Z19 MWT (☆), Z19 pipe (■), YT18 channel DNS (◆), and HJ06 channel DNS (■). Right: values of the profiles on the left taken at $y/\delta \approx 0.1$ (except ASL, see text) versus friction Reynolds number. Symbols as on the left, but with the addition of ASL data from P04 (□ , July 17, 2001 recordings, ☆ , July 25, 2001 recording, ○ , August 3, 2000 recordings.).

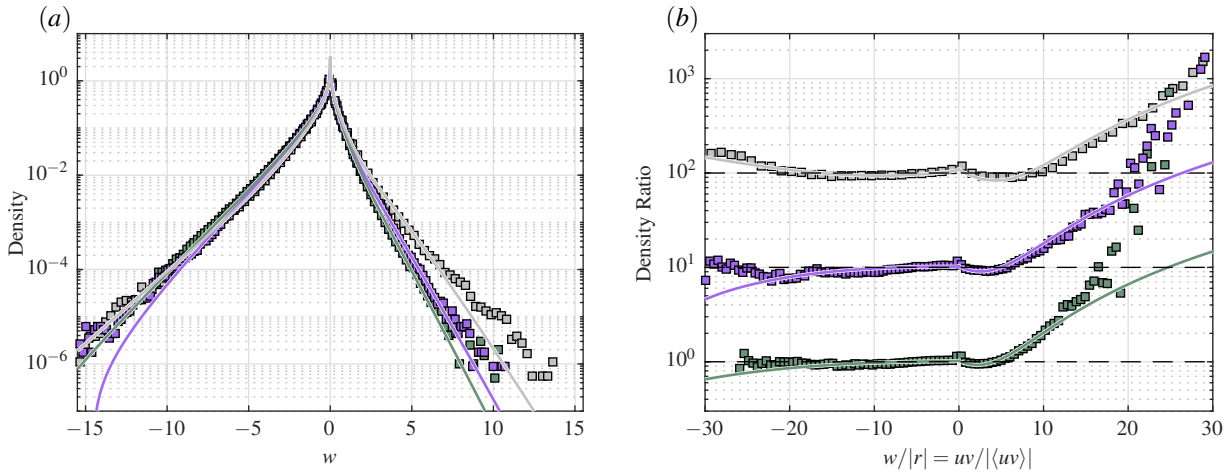

Figure 2. (a): Probability densities of $\delta^+ = 934$ M06 channel DNS (■), $\delta^+ = 7700$ Z19 pipe experiment (■), and $\delta^+ \approx 890,000$ P04 ASL experiment (■). Model equation (1) for each case plotted as solid line with matching color. (b): Same three cases as (a), each divided by the joint-normal product distribution with matching r, vertically shifted for visibility.

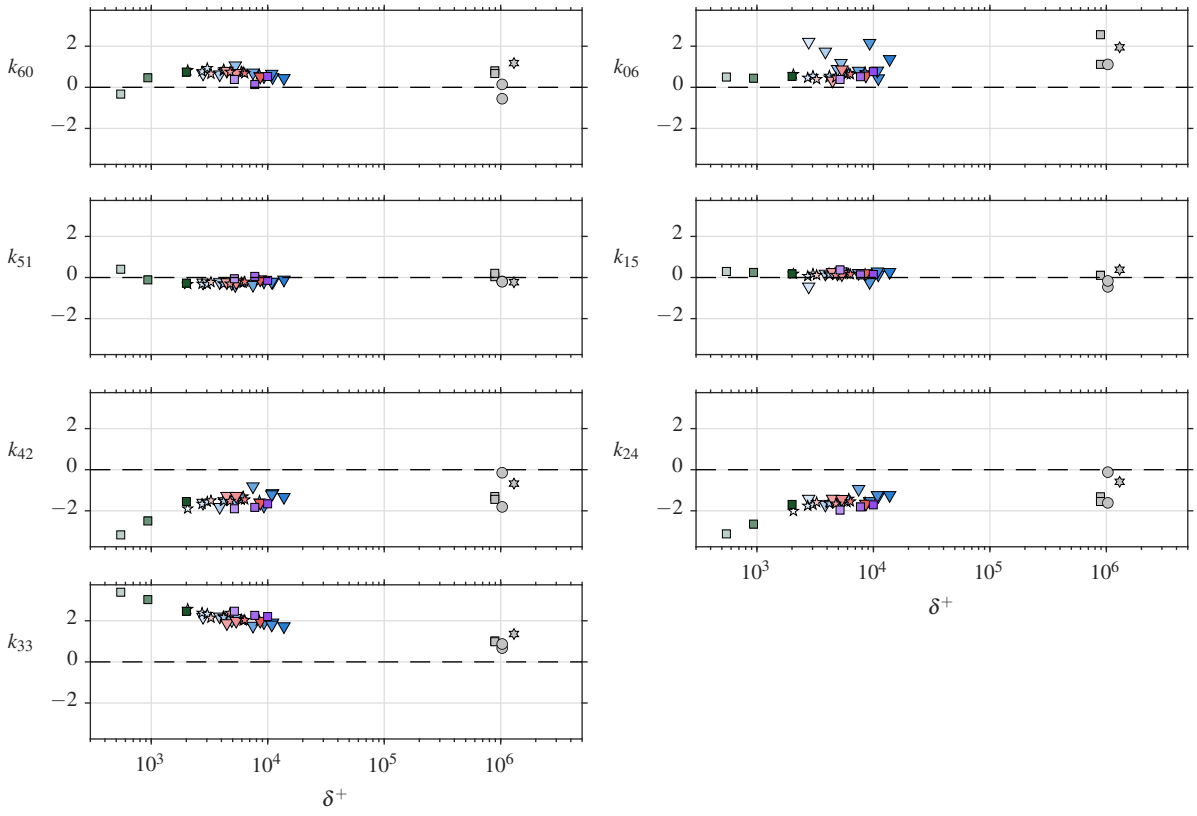

Figure 3. Sixth order joint cumulants of the streamwise and wall-normal velocity at $y/\delta \approx 0.1$ (except ASL, see text) versus friction Reynolds number.

as is the case for the preponderance of the data in figure 1. This can be seen, for example, in the sharp downward turn of the purple model curve in figure 2(a). Expansion to higher orders will presumably resolve this issue along with the failure to describe the density of extremely high magnitude positive events.

Rather than addressing higher order expansions at this time, we instead address the issue of potential invariance in the higher order cumulants in an effort to understand the generality of the result obtained from figure 1. Values of all seven sixth order joint cumulants taken at $y/\delta \approx 0.1$ (or within the overlap layer in the ASL) are plotted in figure 3. Note that these cumulants are not shown in scaled form as were those in figure 1 so that all seven can be plotted on axes with equal

ranges. That being said, these cumulants would also be scaled by $j!k!$ in the higher order expansion, and so note for example that k_{60} would have about 5% as much influence on the distribution as k_{33} of equal magnitude. With this in mind, evidently only k_{42}, k_{24} and k_{33} will substantially affect the higher order model distribution equation. Two former quantities appear to saturate in much the same way as the fourth order cumulants, with most of the variation coming at low Reynolds number as the overlap layer emerges. The values of k_{33} on the other hand appear to be slowly approaching zero, but this observation is unfortunately heavily reliant upon the ASL data in which there is considerable uncertainty. Without them, one could argue that there is just as much of a case for $k_{33} = const.$ as there is for k_{42} or k_{24}, and thus further analysis or measurements are needed before any stronger assertions are possible.

CONCLUSIONS

We have shown that several fourth and sixth order joint cumulants of the streamwise and wall-normal velocity approach non-zero and (in most cases) constant values at the outer edge of the overlap layer of TBL, pipe, and channel flows as Reynolds number increases. Profiles of both fourth and sixth order cumulants (though only the former are shown herein) show that there is very little variation in the magnitudes of these cumulants throughout the entire overlap layer, which allows us to also compare cumulant values from the ASL at smaller y/δ values that are still within the overlap layer. The non-zero asymptotic values are to be expected, as this indicates that the corresponding higher order moments cannot be represented in terms of lower order ones (i.e. it indicates that there is a closure problem in turbulence). The constancy of these cumulants is more interesting, however, as it points to a manifestation of self-similarity/invariance in the overlap layer of several canonical wall-bounded flows. Several cumulants also do appear to be effectively zero relative to others of the same order, indicating that there are no genuine interactions between (for example) u and v^5 or v and u^5, but rather only those that can be explained purely in terms of lower-order interactions.

Although there is clear Reynolds number dependence in the normalized RSS PDF, nearly all of this dependence is attributable to changes in the correlation coefficient r between the streamwise and wall-normal velocities. This fact is *not* due simply to the lack of influence of higher order terms either, as the addition of cumulants up to fourth order captures PDF curvature at low magnitudes and positive tail properties that are not captured by a joint-normal model with matching r.

REFERENCES

Antonia, R.A. & Atkinson, J.D. 1973 High-order moments of Reynolds shear stress fluctuations in a turbulent boundary layer. *J. Fluid Mech.* **58**, 581–593.

Chen, X. & Sreenivasan, K. R. 2022 Law of bounded dissipation and its consequences in turbulent wall flows. *J. Fluid Mech.* **933**, A20.

Del Alamo, J. C. & Jiménez, J. 2003 Spectra of the very large anisotropic scales in turbulent channels. *Phys. Fluids* **15** (6), L41–L44.

Del Alamo, J. C., Jiménez, J., Zandonade, P. & Moser, R. D. 2004 Scaling of the energy spectra of turbulent channels. *J. Fluid Mech.* **500**, 135–144.

Fife, P., Klewicki, J., McMurtry, P. & Wei, T. 2005 Multiscaling in the presence of indeterminacy: wall-induced turbulence. *Multiscale Model. Simul.* **4**, 936–959.

Guala, M., Hommema, S. E. & Adrian, R. J. 2006 Large-scale and very-large-scale motions in turbulent pipe flow. *J. Fluid Mech.* **554**, 521–542.

Hellström, L. H. O. & Smits, A. J. 2017 Structure identification in pipe flow using proper orthogonal decomposition. *Phil. Trans. R. Soc. A* **375** (2089), 20160086.

Hoyas, S. & Jimenez, J. 2006 Scaling the velocity fluctuations in turbulent channels up to $Re_\tau = 2003$. *Phys. Fluids* **18**, 011702.

Isserlis, L. 1918 On a formula for the product-moment coefficient of any order of a normal frequency distribution in any number of variables. *Biometrika* **12** (1/2), 134–139.

Lindgren, B., Johansson, A. V. & Tsuji, Y. 2004 Universality of probability density distributions in the overlap region in high Reynolds number turbulent boundary layers. *Phys. Fluids* **16** (7), 2587–2591.

Marusic, I., Chauhan, K. A., Kulandaivelu, V. & Hutchins, N. 2015 Evolution of zero-pressure-gradient boundary layers from different tripping conditions. *J. Fluid Mech.* **783**, 379–411.

Marusic, I. & Kunkel, G. J. 2003 Streamwise turbulence intensity formulation for flat-plate boundary layers. *Phys. Fluids* **15** (8), 2461–2464.

McKeon, B. J. & Sharma, A. S. 2010 A critical-layer framework for turbulent pipe flow. *J. Fluid Mech.* **658**, 336–382.

Moarref, R., Sharma, A. S., Tropp, J. A. & McKeon, B. J. 2013 Model-based scaling of the streamwise energy density in high-Reynolds-number turbulent channels. *J. Fluid Mech.* **734**, 275–316.

Morrill-Winter, C., Philip, J. & Klewicki, J. 2017*a* An invariant representation of mean inertia: theoretical basis for a log law in turbulent boundary layers. *J. Fluid Mech.* **813**, 594 – 617.

Morrill-Winter, C., Philip, J. & Klewicki, J. 2017*b* Statistical evidence of an asymptotic geometric structure to the momentum transporting motions in turbulent boundary layers. *Phil. Trans. Roy. Soc. A* **375**, 20160084.

Nakagawa, H. & Nezu, I. 1977 Prediction of the contributions to the Reynolds stress from bursting events in open-channel flows. *J. Fluid Mech.* **80**, 99–128.

Perry, A.E. & Chong, M.S. 1982 On the mechanisms of wall turbulence. *J. Fluid Mech.* **119**, 173 – 217.

Priyadarshana, P. J. A 2004 *Reynolds number influences on turbulent boundary layer momentum transport*. PhD Dissertation, University of Utah.

Talamelli, A., Persiani, F., Fransson, J. H. M., Alfredsson, P. H., Johansson, A. V., Nagib, H. M., Rüedi, J.-D., Sreenivasan, K. R. & Monkewitz, P. A. 2009 CICLoPE—a response to the need for high Reynolds number experiments. *Fluid Dyn. Res.* **41** (2), 021407.

Townsend, A. A. 1976 *The Structure of Turbulent Shear Flow*. Cambridge University Press.

Vincenti, P., Klewicki, J. C., Morrill-Winter, C., White, C. M. & Wosnik, M. 2013 Streamwise velocity statistics in turbulent boundary layers that spatially develop to high Reynolds number. *Exp. Fluids* **54** (12), 1–13.

Yamamoto, Y. & Tsuji, Y. 2018 Numerical evidence of logarithmic regions in channel flow at $Re_\tau = 8000$. *Phys. Rev. Fluids* **3**, 012602(R).

Zimmerman, S., Philip, J., Monty, J., Talamelli, A., Marusic, I., Ganapathisubramani, B. . . . & Klewicki, J. 2019 A comparative study of the velocity and vorticity structure in pipes and boundary layers at friction Reynolds numbers up to 10^4. *J. Fluid Mech.* **869**, 182 – 213.